Shear flow in nematic liquid crystals: Fréedericksz transition as a bifurcation

Arup Mukherjee*
Department of Mathematical Sciences, Montclair State University, 1 Normal Avenue, Montclair, New Jersey 07043, USA

Bagisa Mukherjee†
Penn State University, Worthington Scranton Campus, 120 Ridge View Drive, Dunmore, Pennsylvania 18512, USA
(Received 7 May 2004; published 8 February 2005)

We numerically investigate the Fréedericksz transition for steady state plane shear flow of nematic liquid crystals between two parallel plates in the presence of external magnetic fields. Three typical configurations with the external field in the plane of the flow and perpendicular to it, in the plane and along the flow, and where it is perpendicular to the plane of the flow are considered. In each case, the Fréedericksz transition is studied as a bifurcation problem. Beginning with a steady state shear flow, solutions corresponding to slowly increasing magnetic fields and those corresponding to fields which are suddenly turned on at a given intensity are studied. For a typical idealized nematic, we show that the symmetric pitchfork bifurcation in the absence of shear becomes a transcritical bifurcation from the trivial solution in one configuration while in another it resembles a disconnected pitchfork where the turning point of the disconnected branch is a generic singularity in the absence of symmetry or a trivial solution.

DOI: 10.1103/PhysRevE.71.021703 PACS number(s): 61.30.−v, 64.70.Md

I. INTRODUCTION

Nematic liquid crystals exhibit long-range ordering in the sense that their rigid rodlike molecules arrange themselves with their long axes parallel to each other. The direction of alignment is usually described by a unit vector **n** called the director. Mathematical models for nematic liquid crystals are derived generally from the work of Ericksen [1] and Leslie [2]. A comprehensive discussion of the properties of nematic and other liquid crystals can be found in Chandrasekhar [3], deGennes and Prost [4], and Collings and Patel [5].

When an external magnetic field is applied to a nematic liquid crystal trapped between two parallel plates, the base configuration of the liquid crystal changes beyond a critical field value. This effect is called the Fréedericksz transition and is well known. For a thorough discussion see, for example, Ref. [4]. The Fréedericksz transition can be used to measure the elastic constants of a liquid crystal [4, pp. 123-128]. The orienting effect of the applied external field and the anchoring effect of the plates conflict with each other for typical configurations used for the Fréedericksz transition. Leslie [6,7] posed the problem in terms of the conservation of linear and angular momentum and used the free energy of the sample to determine the existence of a critical field strength above which a nontrivial solution can exist. Derfel [8] showed that the critical value above which the transition occurs is at a pitchfork bifurcation point. Blake, Mullin, and Tavener [9] were able to compute the critical value numerically and demonstrate that the perfect pitchfork associated with a magnetic field which is perpendicular to the plate becomes a disconnected pitchfork when the field is slightly perturbed from the perpendicular.

In this paper we investigate the effects described above when a nematic is subject to a steady state shear flow. In particular, we assume that the lower plate is held stationary while the upper plate moves with a constant velocity. We consider three different configurations where the external field and anchoring conditions at the plates are in conflict. In particular, we consider two external fields which are parallel and perpendicular to the flow direction while remaining in the plane of the liquid crystal, and an external field which is perpendicular to the plane of the flow. Our simplifying assumptions reduce the balance laws to a single ordinary differential equation in $\phi(z)$ [or $\theta(z)$], the director angle. We assume that the magnetic properties of the material are anisotropic and the difference of the susceptibilities parallel and perpendicular to the direction of the flow is positive. The material properties of the typical nematic used for numerical investigations is based on Refs. [3,4]. We numerically show that there is a Fréedericksz transition for small shear rates. When the external field is perpendicular to the plane of the liquid crystal, the applied shear plays no role and the observed bifurcation is the perfect pitchfork of the static cases. When the applied field is parallel to the flow direction, we observe a change in the bifurcation picture but it still resembles a pitchfork and the critical field strength changes slightly. In this configuration we obtain a transcritical bifurcation from the trivial solution. However, when the external field is perpendicular to the flow direction and in the plane of the flow, we obtain a disconnected pitchfork at a higher value of the critical field strength. The turning point of the disconnected branch represents a generic singularity in the absence of symmetry.

The rest of the paper is organized as follows. In Sec. II, we outline the continuum theory for nematic liquid crystal flows. Section III describes the Fréedericksz transition and its interpretation as a symmetry breaking bifurcation. Section IV introduces the boundary value problem for the director for steady state shear flows under the influence of a constant

*Electronic address: mukherjeea@mail.montclair.edu
†Electronic address: mukher_b@math.psu.edu

external magnetic field. In Sec. V, we outline the numerical scheme used to solve the boundary value problem. We also demonstrate the effectiveness of our scheme by computing the critical field strength at which nematics undergo Fréedericksz transition and present the symmetry breaking pitchfork bifurcation for this phenomenon. Finally, Sec. VI contains the details of the Fréedericksz transition for nematics under the influence of a shear.

II. DYNAMIC CONTINUUM THEORY FOR NEMATICS

The continuum theory of liquid crystals, established by Ericksen [1,10,11] and Leslie [2], is based on the work of Frank [12] and Oseen [13]. Nematic liquid crystals differ from usual isotropic fluids since they exhibit a long range orientational ordering. Following deGennes and Prost [4, pp. 98-105], we assume the fundamental formula for the bulk free energy of the continuum theory for nematics as

$$\mathcal{F}_{\mathrm{OF}} = \tfrac{1}{2}K_1|\boldsymbol{\nabla}\cdot\mathbf{n}|^2 + \tfrac{1}{2}K_2|\mathbf{n}\cdot(\boldsymbol{\nabla}\times\mathbf{n})|^2 + \tfrac{1}{2}K_3|\mathbf{n}\times(\boldsymbol{\nabla}\times\mathbf{n})|^2, \tag{1}$$

where $K_i>0$, $i=1,2,3$ correspond to the splay, twist, and bend elasticity constants. When $K_1=K_2=K_3=K$ the Oseen-Frank energy reduces to the Dirichlet energy $\mathcal{F}_{\mathrm{Dirichlet}}=K|\nabla\mathbf{n}|^2$ subject to the constraint $|\mathbf{n}|=1$. The formulation does not distinguish between $\mathbf{n}$ and $-\mathbf{n}$. In cgs units, the free energy $\mathcal{F}_{\mathrm{OF}}$ has units of energy (per cm^3) and the elastic constants K_i are expressed in dynes. Different experimental methods used to determine the elastic constants yield different values but their order of magnitude is approximately 10^{-6} dyn.

The equations representing balance laws for mass, linear momentum, and generalized momenta of the anisotropic variables for an incompressible nematic are given below. In addition to $\mathbf{n}$, if we let $\mathbf{v}$ denote the velocity vector, and ρ the density, the balance laws are

$$\boldsymbol{\nabla}\cdot\mathbf{v} = 0, \tag{2}$$

$$\rho\dot{\mathbf{v}} = \boldsymbol{\nabla}\cdot\sigma, \tag{3}$$

$$\gamma_1\dot{\mathbf{n}}\times\mathbf{n} = \boldsymbol{\nabla}\cdot\left(\frac{\partial\mathcal{F}_{\mathrm{OF}}}{\partial\boldsymbol{\nabla}\mathbf{n}}\right)\times\mathbf{n} - \frac{\partial\mathcal{F}_{\mathrm{OF}}}{\partial\mathbf{n}}\times\mathbf{n} + \gamma_1\boldsymbol{\Omega}\mathbf{n}\times\mathbf{n} - \gamma_2\mathbf{A}\mathbf{n}\times\mathbf{n}. \tag{4}$$

In the above equations, the Cauchy stress tensor σ is given by

$$\sigma = pI - \boldsymbol{\nabla}\mathbf{n}^T\frac{\partial\mathcal{F}_{\mathrm{OF}}}{\partial\boldsymbol{\nabla}\mathbf{n}} + \sigma_v, \tag{5}$$

where the viscous stress σ_v is defined as

$$\sigma_v = (\alpha_1\mathbf{n}\cdot\mathbf{A}\mathbf{n})\mathbf{n}\otimes\mathbf{n} + \alpha_2\mathbf{N}\otimes\mathbf{n} + \alpha_3\mathbf{n}\otimes\mathbf{N} + \alpha_4\mathbf{A} + \alpha_5\mathbf{A}\mathbf{n}\otimes\mathbf{n} + \alpha_6\mathbf{n}\otimes\mathbf{A}\mathbf{n}. \tag{6}$$

The tensors $\mathbf{A}$ and $\boldsymbol{\Omega}$ represent the symmetric and skew-symmetric parts of the velocity gradient, $\mathbf{N}=\dot{\mathbf{n}}-\boldsymbol{\Omega}\mathbf{n}$ is an invariant time derivative of $\mathbf{n}$, $\dot{\mathbf{n}}$, and $\dot{\mathbf{v}}$ denote material time derivatives, and $p(\mathbf{x},t)$ is the pressure. The six Leslie coefficients α_i determine the dynamics of the incompressible nematic and the constants γ_1 and γ_2 are linear combinations of the α_i's. For the few cases where experimental determination is possible, these coefficients are of comparable magnitude and in cgs units they range in value from 10^{-2} to 10^{-1} P.

A magnetic field $\mathbf{H}$ making an arbitrary angle with the director $\mathbf{n}$ induces the magnetization $\mathbf{M}$ given by

$$\mathbf{M} = \chi_\perp\mathbf{H} + (\chi_\parallel - \chi_\perp)(\mathbf{H}\cdot\mathbf{n})\mathbf{n} = \chi_\perp\mathbf{H} + \chi_a(\mathbf{H}\cdot\mathbf{n})\mathbf{n}, \tag{7}$$

where χ_a measures the difference between the magnetic susceptibilities parallel and perpendicular to the director and is positive for typical nematics. In cgs electromagnetic units, χ_a is approximately equal to 10^{-7}. The magnetic torque $\boldsymbol{\Gamma}_{\mathbf{M}}$ acting on the magnetization $\mathbf{M}$ is $\boldsymbol{\Gamma}_{\mathbf{M}}=\mathbf{M}\times\mathbf{H}=\chi_a(\mathbf{n}\cdot\mathbf{H})\mathbf{n}\times\mathbf{H}$. To include the effect of a magnetic field $\mathbf{H}$, we modify the free energy $\mathcal{F}_{\mathrm{OF}}$ of Eq. (1) to

$$\mathcal{F} = \mathcal{F}_{\mathrm{OF}} - \int_0^H \mathbf{M}\cdot d\mathbf{H} = \mathcal{F}_{\mathrm{OF}} - \frac{1}{2}\chi_\perp H^2 - \frac{1}{2}\chi_a(\mathbf{n}\cdot\mathbf{H})^2, \tag{8}$$

where $H=\|\mathbf{H}\|$. The term $\frac{1}{2}\chi_\perp H^2$ is independent of the molecular orientation $\mathbf{n}$ and does not play a part in our discussion, while the last term in the expression for $\mathcal{F}$ is minimized when $\mathbf{n}$ and $\mathbf{H}$ are collinear, since $\chi_a>0$. The balance laws in the presence of an external magnetic field are given by the Ericksen-Leslie equations (2)–(4) where $\mathcal{F}_{\mathrm{OF}}$ is replaced by $\mathcal{F}$. We study the Fréedericksz transition for nematic liquid crystals under the influence of a plane shear and an uniform magnetic field. The boundary value problem for the director orientation under these assumptions is derived in Sec. IV.

III. FRÉEDERICKSZ TRANSITION

The simplest method for determining the elastic constants K_i is by studying the deformations of a thin layer of nematic between two plates due to an external magnetic field [14,15]. Three typical experimental configurations of a nematic between two plates, a distance d apart, are shown in Fig. 1. The thin nematic slice is in the xz plane and the geometries are chosen so that the orienting effect of the applied external field competes with the restoring forces produced by the director alignment at the boundaries. As shown in the figure, $\phi=\phi(z)$ and $\theta=\theta(z)$ are the angles that the director $\mathbf{n}$ makes with the x and z axis with $\phi+\theta=\pi/2$ and H represents the constant external magnetic field. Specific details for the three configurations including the boundary value problem for the director angle θ or ϕ are given below.

Configuration (a). The undisturbed director orientation is parallel to the plates and the applied magnetic field acts perpendicular to the plate in the xz plane. Using $\mathbf{n}=(\cos\phi,0,\sin\phi)$, $\mathbf{H}=(0,0,H)$, and $\mathbf{v}=(0,0,0)$ in Eqs. (2)–(4) and (8), we obtain

$$f_a(\phi)\frac{d^2\phi}{dz^2} + \frac{1}{2}\frac{df_a}{d\phi}\left[\frac{d\phi}{dz}\right]^2 = -\frac{\chi_a H^2}{2}\sin 2\phi, \tag{9}$$

with the strong anchoring boundary conditions $\phi(-d/2)=\phi(d/2)=0$, where $f_a(\phi)=K_1\cos^2\phi+K_3\sin^2\phi$. The mag-

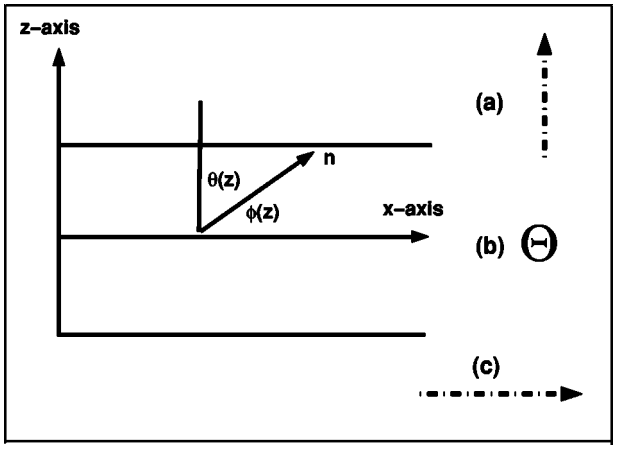

FIG. 1. Model configurations for Fréedericksz transition. Configurations (a), (b), and (c)represent different geometries and the broken arrows or Θ shows the direction of the external magnetic field H.

netization $\mathbf{M}=[(\chi_a H/2)\sin 2\phi, 0, \chi_\perp H+\chi_a H \sin^2\phi]$, and the magnetic torque $\mathbf{\Gamma_M}=(0,-(\chi_a H^2/2)\sin 2\phi, 0)$.

Configuration (b). The undisturbed director orientation is parallel to the plates and the applied magnetic field acts perpendicular to the xz plane. Using $\mathbf{n}=(\cos\phi, \sin\phi, 0)$, $\mathbf{H}=(0,H,0)$, and $\mathbf{v}=(0,0,0)$ in Eqs. (2)–(4) and (8), we obtain

$$K_2\frac{d^2\phi}{dz^2}=-\frac{\chi_a H^2}{2}\sin 2\phi \tag{10}$$

with $\phi(-d/2)=\phi(d/2)=0$. The magnetization $\mathbf{M}=((\chi_a H/2)\sin 2\phi, \chi_\perp H+\chi_a H\sin^2\phi, 0)$, and the magnetic torque $\mathbf{\Gamma_M}=(0,0,(\chi_a H^2/2)\sin 2\phi)$.

Configuration (c). The undisturbed director orientation is perpendicular to the plates and the applied magnetic field acts parallel to the plates (or perpendicular to the undisturbed director orientation). Using $\mathbf{n}=(\sin\theta, 0, \cos\theta)$, $\mathbf{H}=(H,0,0)$, and $\mathbf{v}=(0,0,0)$ in Eqs. (2)–(4) and (8), we obtain

$$f_c(\theta)\frac{d^2\theta}{dz^2}+\frac{1}{2}\frac{df_c}{d\theta}\left[\frac{d\theta}{dz}\right]^2=-\frac{\chi_a H^2}{2}\sin 2\theta, \tag{11}$$

with the strong anchoring boundary conditions $\theta(-d/2)=\theta(d/2)=0$, where $f_c(\theta)=K_1\sin^2\theta+K_3\cos^2\theta$. The magnetization $\mathbf{M}=(\chi_\perp H+\chi_a H\sin^2\theta, 0, (\chi_a H/2)\sin 2\theta)$ and the magnetic torque $\mathbf{\Gamma_M}=(0,(\chi_a H^2/2)\sin 2\theta, 0)$.

Configuration (b) is the simplest since it involves only the twist constant K_2. If we assume $K_1=K_3=K$, then the equations for configurations (a) and (c) simplify, since $f_a(\phi)=f_c(\theta)=K$ and $df_a/d\phi=df_c/d\theta=0$. Using these assumptions, introducing a new scaled variable $\tilde{z}=z/d$ and using primes to denote derivatives with respect to the normalized variable, we arrive at the generic boundary value problem

$$u''=-\lambda\sin 2u, \quad \text{with } u(-1/2)=u(1/2)=0, \tag{12}$$

where $\lambda=\chi_a H^2 d^2/2K$, and u is either ϕ or θ.

The competition between the effects of the field and the restoring forces of the boundary alignment leads to transition layers near the plates where the molecular effects have a complicated coupling with the field. Following deGennes and Prost [4, pp. 122-123], the magnetic coherence length of a nematic is defined as $\xi(\mathbf{H})=(1/H)(K/\chi_a)^{1/2}$ where we have assumed $K_1=K_2=K_3=K$. It is well known that the thickness of the transition layer is essentially equal to the magnetic coherence length. In cgs units, taking $K=10^{-6}$, $\chi_a=10^{-7}$, and $H=10^4$ Oe, we notice that $\xi(\mathbf{H})$ has the order of 10^{-4} cm or 1 μm. If the sample thickness d is much larger than $\xi(\mathbf{H})$, the bulk of the sample tends to align in the field direction.

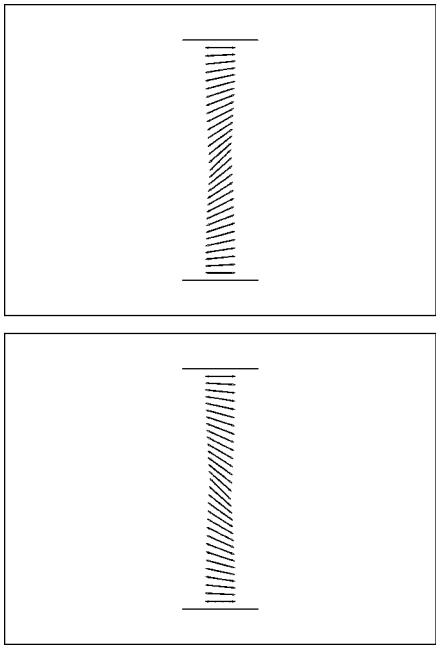

FIG. 2. Typical anticlockwise (top) and clockwise (bottom) distortions of the director measured with respect to $\phi=0$. For θ, the orientations are reversed.

The trivial solution always solves the boundary value problems (9)–(11) and there is a critical field strength H_c above which the magnetic torque overcomes the restoring elastic forces and the director profile becomes distorted. The critical field strength is

$$H_c=\frac{\pi}{d}\left(\frac{K}{\chi_a}\right)^{1/2} \text{ or } \lambda_c=\frac{\pi^2}{2}. \tag{13}$$

Blake, Mullin, and Tavener [9] study this problem as a symmetry breaking (pitchfork) bifurcation. They assume $\mathbf{H}=(H\sin\psi, 0, H\cos\psi)$ and discuss the two cases $\psi=0$ [their computations correspond to configuration (a) in this case] and $\psi\neq 0$. The inherent reflectional symmetry of the problem when $\psi=0$ is broken when ψ is nonzero. They show that for $H>H_c$, two nontrivial solutions corresponding to clockwise and anticlockwise distortions of the director appear. Typical anticlockwise and clockwise distortions of the director with respect to $\phi=0$ are shown in Fig. 2. The graph of $\phi(z)$, $-d/2\leq z\leq d/2$ has the shape of a flattened parabola opening downwards for anticlockwise distortions while it opens upwards for clockwise orientations. The parabola becomes flatter and its vertex approaches the values $\pm\pi/2$ as λ increases. If the graph of $\theta(z)$, $-d/2\leq z\leq d/2$ has a parabolic shape

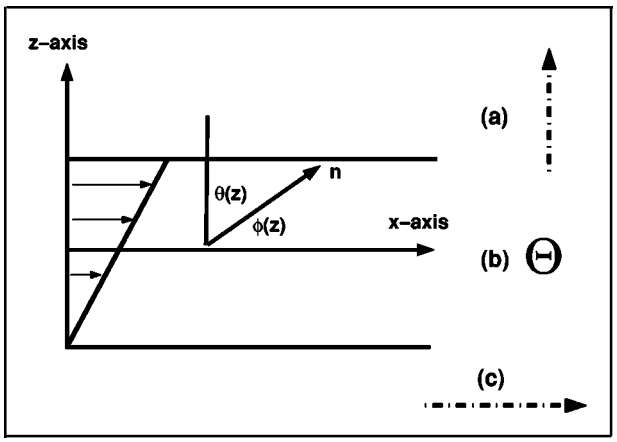

FIG. 3. Model configurations for shear flow. The lower plate is stationary and the upper plate has constant velocity V/d.

opening upward (respectively downward), then this curve corresponds to anticlockwise (respectively clockwise) distortion with respect to $\theta=0$ or $\phi=\pi/2$. As the field strength is increased steadily beyond H_c, the trivial solution exchanges stability with one or two possible nontrivial solutions which are equally likely to occur leading to a pitchfork bifurcation. Beyond the critical value, the trivial solution is unstable and the distorted branches approach $\pm\pi/2$ as $H\to\infty$. When $\psi \neq 0$, the trivial solution no longer solves the boundary value problem and there is a distortion in the director for any field strength. Moreover, the bifurcation becomes a disconnected pitchfork with a primary and a secondary branch.

IV. PLANE SHEAR FLOW FIELDS

We consider boundary value problems for a class of one dimensional steady state shear flows between two parallel plates. Figure 3 shows three typical configurations in the case where the flow is along the positive x axis. Using $\mathbf{v}=(v(z),0,0)$ in the balance laws, the boundary value problems for the three standard configurations are only slightly modified from the static cases discussed in the previous section. In particular, the differential equation (9) for configuration (a) now has the additional term $\frac{1}{2}(dv/dz)(\gamma_1+\gamma_2\cos 2\phi)$ on the right, Eq. (10) is unchanged, and Eq. (11) for configuration (c) acquires the additional term $\frac{1}{2}(dv/dz)\times(\gamma_2\cos 2\theta-\gamma_1)$ on the right. Notice that for configuration (b) the addition of a shear does not change the boundary value problem for determining the director. Thus the critical field strength in this case will be $\lambda_c=\pi^2/2\approx 4.93$.

Assuming that the upper plate moves at a constant rate of V/d in the direction of increasing x, $v(z)=(V/d)(z+d/2)$, or $dv/dz=V/d$. Introducing a new scaled variable $\tilde{z}=z/d$, replacing γ_1 and γ_2 by some average γ, and assuming that the elastic constants K_1 and K_3 are equal to K, we arrive at the normalized boundary value problems

$$\phi''=-\lambda\sin 2\phi+\mu(1+\cos 2\phi) \tag{14}$$

with $\phi(-1/2)=\phi(1/2)=0$ for configuration (a),

$$\phi''=-\lambda\sin 2\phi \text{ with } \phi(-1/2)=\phi(1/2)=0 \tag{15}$$

for configuration (b), and

$$\theta''=-\lambda\sin 2\theta+\mu(\cos 2\theta-1) \tag{16}$$

with $\theta(-1/2)=\theta(1/2)=0$ for configuration (c), where $\mu=Vd\gamma/2K$. The trivial solution still solves Eqs. (15) and (16), but every solution for configuration (a) with $\mu\neq 0$ corresponds to a distortion of the director.

V. NUMERICAL TECHNIQUES

In this section, we present the numerical techniques used to solve boundary value problems of the form (14)–(16) for the director orientation $\phi(z)$ or $\theta(z)$ on the domain $-1/2\leqslant z\leqslant 1/2$. Two point boundary value problems can be written in standard form as a first order system,

$$\mathbf{y}'(z)=\mathbf{f}(z,\mathbf{y}(z)) \text{ on } a\leqslant z\leqslant b, \tag{17}$$

$$\text{with } \mathbf{g}(\mathbf{y}(a),\mathbf{y}(b))=\mathbf{0}, \tag{18}$$

where $\mathbf{y}$, $\mathbf{f}$, and $\mathbf{g}$ have n components and both $\mathbf{f}$ and $\mathbf{g}$ may be nonlinear (see, for example, Ascher and Russel [16]). For the single second order equation we consider here, $n=2$. There is a comprehensive body of work on efficient numerical methods for boundary value problems of the form (17) with boundary conditions (18). For an overview on available codes and their interrelations, consider Shampine, Gladwell, and Thompson [[17], pp. 156–167]. The book by Ascher, Mattheij, and Russell [18] contains a more comprehensive study and analysis of the numerical methods relevant to two-point boundary value problems.

A robust approach for solving the boundary value problem (17) and (18) is to choose a form of the approximate solution involving unknown parameters, require that this approximating function satisfies the boundary conditions (18), and then use collocation at a sufficient number of points so that the parameters are determined uniquely. In particular, if $a=z_0<z_1<z_2<\cdots<z_N=b$ is a mesh on $[a,b]$, the boundary value problem can be solved by computing a cubic function $S(z)$ on each subinterval $[z_i,z_{i+1}]$. The coefficients of the function $S(z)$ are determined by requiring that $S(z)\in C[a,b]$, $g(S(a),S(b))=0$, and that the piecewise cubic satisfy Eq. (17) at both endpoints and the midpoint of each subinterval. These conditions result in a system of nonlinear algebraic equations in the coefficients of the piecewise cubic function $S(z)$ and it can be shown that $S(z)\in C^1[a,b]$. Once a good guess of the solution is available on the initial mesh, we use collocation to find an approximate solution on this mesh, use an error estimator to estimate the error on each subinterval, refine the mesh as indicated by the error estimator, and then solve the problem on the resulting finer mesh. This iterative process is repeated until the difference in the computed solutions on two successive meshes or some similar stopping criterion meets a predetermined error tolerance. The error estimator used for adaptive mesh refinement requires specialized techniques. We use a Richardson extrapolation based error estimator for our computations. The computed solution $S(z)$ satisfies the equation

$$S'(z) = \mathbf{f}(z, S(z)) + r(z), \tag{19}$$

where $r(z)$ is the residual. For each subinterval $[z_i, z_{i+1}]$ of any mesh, we associate a residual error estimator $r(i) = \int_{z_i}^{z_{i+1}} \|r(z)\|^2 dz$, where the integral is evaluated using a five-point Lobatto quadrature formula. We use a stopping criterion where on each subinterval of the final mesh, the residual satisfies

$$\left\| \frac{r(i)}{\max\left(|\mathbf{f}(i)|, \frac{A(i)}{R} \right)} \right\| \leq R, \tag{20}$$

where R is the relative tolerance and $A(i)$ is the absolute tolerance on $[z_i, z_{i+1}]$. For our computations, we choose $R = 10^{-2}$ and $A(i) = 10^{-5}$. We have checked all the numerical results we report in this work with lower values of the tolerances and with a finer final mesh than the one we use for our results in the paper. The difference between the reported values and the more accurate ones are insignificant.

When the boundary value problem (17) is difficult to solve, the method of continuation is commonly used. The technique exploits the fact that the solution of one boundary value problem is a good guess for another whose parameters differ only slightly. For example, we can solve any of the boundary value problems (14)–(16) for given values of λ and μ by using a continuation on λ as follows. Introduce a parameter δ into the first term of the boundary value problem and solve for $\delta = 0$ (correspondingly $\lambda = 0$). Using the solution of this problem, solve successive boundary value problems for $0 < \delta_1 < \delta_2 < \cdots < \delta_M = 1$. The final solution solves the problem for the given parameters λ and μ. We have implemented these numerical methods using the available tools and functionality of MATLAB. A detailed discussion of the numerical analysis and control of bifurcations in boundary value problems can be found in Doedel, Keller, and Kernévez [19,20].

Given particular values of the parameters λ and μ, we solve the boundary value problem using two different approaches. In the first approach the solution is obtained using continuation on the magnetic field parameter λ. This corresponds to an experiment where we start with a given flow rate and no magnetic field and slowly ramp up the magnetic field to its desired value—we will refer to this as the *ramped field*. The process of starting at the initial value $\lambda_i > 0$, of the parameter λ and reaching a final value λ_f with $\lambda_f < \lambda_i$ using continuation will be called downward ramping. When continuation is not used, the solution scheme corresponds to a sudden application of the magnetic field at the given intensity. We will refer to this as an *impulse field*. Notice that the equations we solve are pure boundary value problems and our reference to impulse fields is just a way to distinguish between the two methods of solving these boundary value problems.

All computations in the next section correspond to three different forms of the initial guess for $\phi(z)$ [respectively $\theta(z)$] which satisfy the boundary values. The three initial guesses used for our computations are as follows:

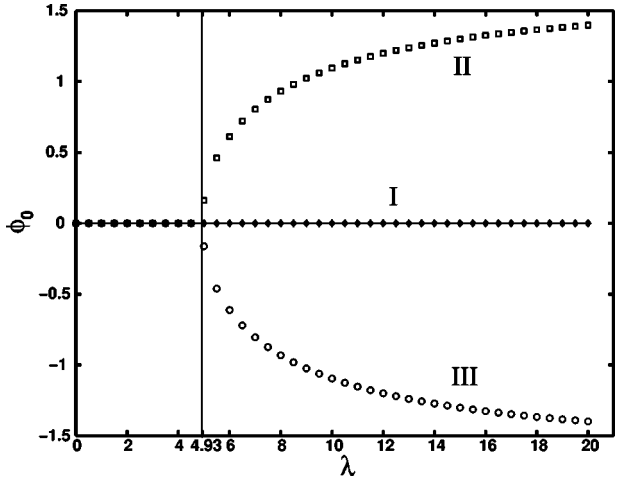

FIG. 4. Computed bifurcation diagram for the Fréedericksz transition with shear in configuration (b) corresponding to the boundary value problem (12). ◇, □, and ○ indicate impulse field computations with initial guesses corresponding to I, II, and III, respectively. The line along the trivial branch indicates that ramped field computations corresponding to I, II, and III yield this solution branch.

Branch I. The undistorted orientation corresponding to $\phi(z) \equiv 0$ [respectively $\theta(z) \equiv 0$].

Branch II. The positive orientation corresponding to $\phi(z) = \phi_0 \cos(\pi z)$ [respectively $\theta(z) = \theta_0 \cos(\pi z)$]. This initial guess assumes an initial anticlockwise (respectively clockwise) distortion.

Branch III. The negative orientation corresponding to $\phi(z) = -\phi_0 \cos(\pi z)$ [respectively $\theta(z) = -\theta_0 \cos(\pi z)$]. This initial guess assumes an initial clockwise (respectively anticlockwise) distortion.

For most of our computations we assume $\phi_0 = 1$. These choices are motivated by approximations of the boundary value problems as shown below.

A. Choice of initial configurations

A first order approximation for the differential equation (14) yields

$$\phi'' = -\lambda \sin 2\phi + \mu(1 + \cos 2\phi) \approx -2\lambda\phi + 2\mu \tag{21}$$

with $\phi(-1/2) = \phi(1/2) = 0$. Assuming $\phi(z) = C\cos(\pi z)$ for the solution, we obtain $C = \phi_0 = \phi(0)$. Thus the solution to the approximate boundary value problem (21) yields anticlockwise (respectively clockwise) distortions depending on the sign of ϕ_0. Substituting this form of the solution in Eq. (21) yields $\phi_0 \cos \pi z = 2/(2\lambda - \pi^2)$. This immediately leads to the critical values $\lambda_c = \pi^2/2$ where the solution changes nature. We have used this first order approximate solution to the boundary value problem (14) as the initial guess for our numerical computations. The three solution branches in our bifurcation diagrams correspond to $\phi_0 = 0$, $\phi_0 > 0$, and $\phi_0 < 0$.

B. Fréedericksz transition as a bifurcation

As a partial validity of our computational methods, Fig. 4 shows the computed bifurcation diagram for the boundary

value problem (12) when $0 \leqslant \lambda \leqslant 20$. This corresponds to any of the three configurations in Sec. IV or to the shear flow configuration (b). The ramped field computations always corresponds to the trivial solution branch as indicated by the line along this branch, even when $\lambda > \lambda_c = \pi^2/2$. On the other hand, the impulse field computations yield the trivial solution when $\lambda < \lambda_c$ and the corresponding nontrivial solution branch when $\lambda > \lambda_c$. Figure 4 shows all three solution branches as plots of $\phi_0 = \phi(0)$ [respectively $\theta_0 = \theta(0)$] against the parameter $\lambda = \chi_a H^2 d^2/2K$. For the nontrivial solution branches, the variables ϕ (respectively θ) always attain their maximum value at $z=0$. These observations match the findings of Blake, Mullin, and Tavener [9] who use a finite element approach based on the package Entwife [21] to solve the boundary value problems and compute the critical value λ_c. Derfel [8] first showed that the static Fréedericksz transition that occurs when a magnetic field is applied normal to the nematic [static configuration (a)] arises at a pitchfork bifurcation point.

VI. DISCUSSION AND RESULTS

We consider an idealized nematic with the following material characteristics (in cgs units):

(i) the difference between the magnetic susceptibilities is approximately 10^{-7}, or $\chi_a \sim 10^{-7}$;

(ii) the elastic constants are equal to $K \sim 10^{-6}$;

(iii) the viscosity constants γ_1 and γ_2 are assumed to be replaced by some average $\gamma \sim 10^{-1}$.

Justifications for the orders of magnitude and underlying assumptions for the material characteristics follow from our discussions in Secs. II and III. Further, the plate separation d is assumed large enough so that boundary effects may be ignored. To this end, we take d to be of the order of 30–80 μm or 10^{-3} cm. Following purely dimensional arguments, if we assume a slow normalized shear rate V of approximately 10^{-2} for the upper plate and a large applied external magnetic field $H \sim 10^4$, the assumptions underlying the model of Sec. III are justified. With these choices the magnetic coherence length turns out to be smaller than the plate separation d, or equivalently, $10^4 \sim H \gg (1/d)\sqrt{(K/\chi_a)} \sim 10^3$. The unperturbed alignment condition derived from a balance of the magnetic and shear induced hydrodynamic torques, $10^{-2} \sim V \ll (\chi_a H^2)/\gamma \sim 10^2$ is also satisfied. For these parameter choices the constants μ and λ are approximately

$$\mu = \frac{Vd\gamma}{2K} \sim \frac{10^{-2}10^{-3}10^{-1}}{2\times 10^{-6}} \sim 1 \text{ and} \tag{22}$$

$$\lambda = \frac{\chi_a H^2 d^2}{2K} = \frac{10^{-7}10^{8}10^{-6}}{2\times 10^{-6}} \sim 10. \tag{23}$$

Notice that choosing $\gamma \sim 10^{-2}$ and $V \sim 10^{-1}$ does not change the estimated values of λ or μ above. Shear configuration (b) was discussed in the previous section and our observations for the other configurations are presented below.

A. Bifurcation for shear configuration (c)

Figure 5 shows the bifurcation diagram for configuration (c) in the presence of a steady state shear where we have assumed $\mu = 1$. Although Figs. 5 and 4 look similar, there are many differences. Equation (16) does not have any symmetry but admits a trivial solution and Fig. 5 is an example of a transcritical bifurcation from the trivial solution. Moreover, the value of λ_c is only approximately $\pi^2/2$. Our numerical experiments suggest that the upper branch II breaks off from the trivial solution I at a slightly lower value of λ than the lower branch III. A detailed study of the structure near these critical values was not attempted in this work.

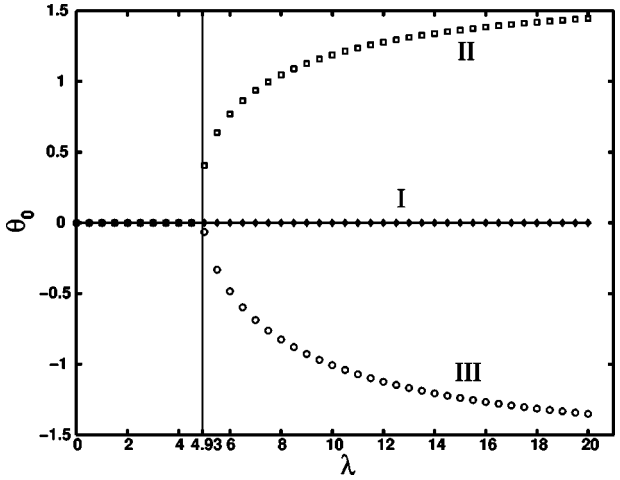

FIG. 5. Computed bifurcation diagram for the Fréedericksz transition with shear in configuration (c) corresponding to the boundary value problem (16). ◇, □, and ○ indicate impulse field computations with initial guesses corresponding to I, II, and III, respectively. The line along the trivial branch indicates that ramped field computations corresponding to I, II, and III all yield this solution branch.

Computations for impulse fields with initial guesses $\theta(z) = 0$, $\cos(\pi z)$, and $-\cos(\pi z)$, are shown using ◇'s, □'s, and ○'s, respectively. The corresponding solution branches are marked as I, II, and III. The continuous line along the trivial branch indicates that all upward ramped field computations lie along this branch. If we start on any solution branch at some nonzero value of λ_i, and use downward ramping to reach a value $0 < \lambda_f < \lambda_i$, the solution never leaves the branch. Since $\theta(z)$ represents the angle the director makes with the z axis as shown in Fig. 1, solutions along branch II (respectively III) represent clockwise (respectively anticlockwise) distortions of the director from the undistorted configuration where the directors are perpendicular to the plates, or $\theta \equiv 0$.

B. Bifurcation for configuration (a)

Figure 6 shows the bifurcation diagram for configuration (a) in the presence of a steady state shear with $\mu = 1$. The trivial solution no longer solves the boundary value problem (14), and every value of the magnetic field strength parameter λ yields a distortion. Derfel [8], investigating the effects of imperfect alignment at the plates when a magnetic field is applied normal to a static nematic, and the effects of the magnetic field deviating slightly from normal, found similar disconnected pitchforks. Blake, Mullin, and Tavener [9] also obtain a similar bifurcation picture by considering the nem-

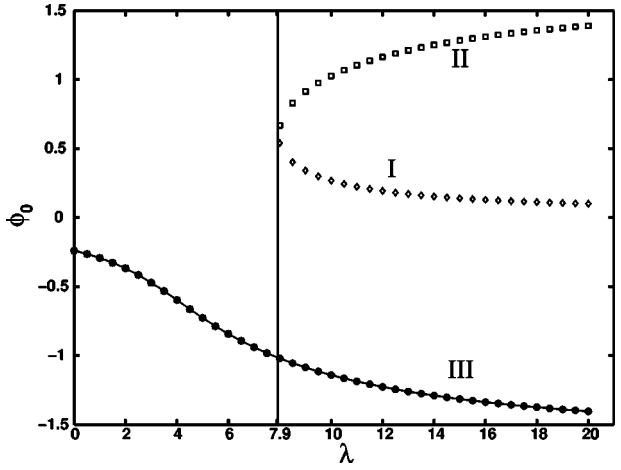

FIG. 6. Computed bifurcation diagram for the Fréedericksz transition with shear in configuration (a) corresponding to the boundary value problem (14). ◇, □, and ○ indicate impulse field computations with initial guesses corresponding to I, II, and III, respectively. The line along the lower branch indicates that ramped field computations corresponding to I, II, and III all yield this solution branch. The initial guesses are $\phi(z)=\pm\cos(\pi z)$ or $\phi(z)=0$.

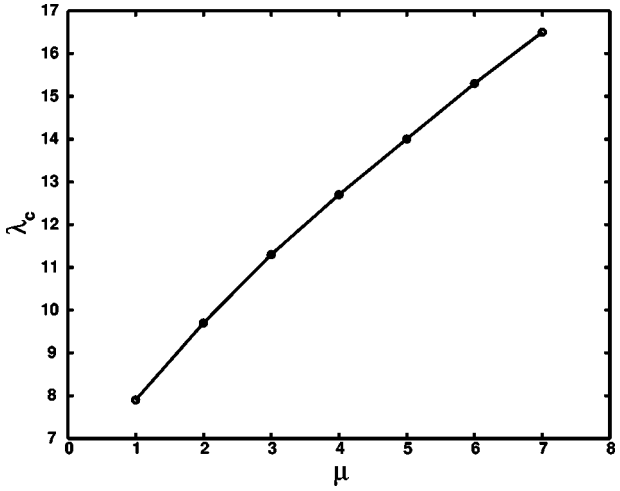

FIG. 7. Relationship between λ_c and $\mu=Vd\gamma/2K$ for configuration (a).

atic configuration (a) without any flow, and assuming the magnetic field to be $\mathbf{H}=(H\sin\psi,0,H\cos\psi)$, where ψ represents the deviation of the magnetic field from the normal to the nematic. Their bifurcation diagram is a reflection in the λ axis of Fig. 6.

The lower branch of the bifurcation diagram represents impulse field computations, indicated by the ○'s, corresponding to the negative initial distortions for branch III. Moreover, the line in Fig. 6 represents ramped field computations beginning at $\lambda_i=0$ and continuing upward to $\lambda_f>0$ for initial distortions corresponding to I, II, and III. This suggests that the stability of the trivial solution in the symmetric pitchfork of configuration (b) is transferred to this lower branch. Moreover, $\phi_0=\phi(0)=\min_{[-1/2,1/2]}\phi(z)$ approaches $-\pi/2$ as $\lambda\to\infty$.

A nematic between two plates under a steady shear and with no magnetic field has a clockwise distortion in ϕ as indicated by the value of $\phi_0=\phi(0)\approx-0.25$ corresponding to $\lambda=0$ in Fig. 6. Since all solutions for ramped fields lie on the lower branch in Fig. 6, we infer that the applied external ramped fields are unable to overcome the effects of the shear and the anchoring at the plates. Our numerical experiments demonstrate that this changes when a slightly different initial condition which preserves the shape is chosen. In practice, a Fréedericksz transition experiment including shear may involve imposing the steady state shear on the sample before the magnetic field is turned on. We have found that ramped field computations corresponding to an initial clockwise configuration $\phi(z)=-0.25\cos(\pi z)$ always remain on the lower branch, while the impulse field computations corresponding to the same initial guess switch from branch III to branch I beyond $\lambda=\lambda_c$.

The upper portion of the bifurcation picture in Fig. 6 consists of the two branches I and II represented by ◇'s and □'s, respectively. Branch I corresponds to impulse field computations for undistorted initial configurations. Impulse fields with undistorted initial guesses jump from the lower branch to branch I at $\lambda_c\approx7.9$. Impulse field computations corresponding to the initial guess $\phi(z)=\cos(\pi z)$ have a similar behavior as they switch from the lower branch to branch II. A solution stays on branch I (respectively II) for $\lambda>\lambda_c$ when downward ramping is employed starting with $\lambda_i=20$, and switches to the lower branch for $\lambda<\lambda_c$. The value of λ_c is independent of the initial configurations used. Thus the transition at λ_c may occur for any of the three initial orientations of the director and we can view the turning point in Fig. 6 as a generic singularity in the absence of both symmetry and a trivial solution.

Since μ is directly proportional to both the normalized shear rate V and the plate separation d, increases in the parameter μ can be viewed as increasing either the normalized shear rate or the separation between the plates. Changing the value of the parameter μ changes the values λ_c without changing the qualitative behavior of the Fréedericksz transition for shear flows. Figure 7 shows the relationship between λ_c and μ for $1\leqslant\mu\leqslant7$.

VII. CONCLUSIONS

We have carefully investigated the Fréedericksz transition in steady state plane shear flows of nematic liquid crystals between two parallel plates. We show numerically that when the applied magnetic field is in the plane of the flow and along the direction of the flow, the critical field strength at which the transition occurs is close to the critical value in the absence of flow. However, the perfect pitchfork bifurcation obtained in the absence of flow is replaced by a transcritical bifurcation from the zero solution. We also demonstrate that when the applied magnetic field is perpendicular to the flow direction, the Fréedericksz transition occurs at a higher value and the bifurcation resembles a disconnected pitchfork. The director orientation is sensitive to how the external field is changed and the initial orientation of the director, but we demonstrate the occurrence of the Fréedericksz transition for initial configurations corresponding to both anticlockwise

and clockwise distortion of the director in the presence of shear.

[1] J. L. Ericksen, Arch. Ration. Mech. Anal. **4**, 231 (1960).
[2] F. M. Leslie, Adv. Liq. Cryst. **4**, 1 (1979).
[3] S. Chandrasekhar, *Liquid Crystals* (Cambridge University Press, Cambridge, England, 1992).
[4] P. G. de Gennes and J. Prost, *The Physics of Liquid Crystals* (Clarendon Press, Oxford, 1993).
[5] P. J. Collings and J. Patel, *Handbook of Liquid Crystal Research* (Oxford University Press, New York, 1997).
[6] F. M. Leslie, Mol. Cryst. Liq. Cryst. **12**, 57 (1970).
[7] F. M. Leslie, J. Phys. D **3**, 889 (1970).
[8] G. Derfel, Liq. Cryst. **93**, 1411 (1988).
[9] G. I. Blake, T. Mullin, and S. J. Tavener, Dyn. Stab. Syst. **14**, 299 (1999).
[10] J. L. Ericksen, Trans. Soc. Rheol. **5**, 23 (1961).
[11] J. L. Ericksen, Arch. Ration. Mech. Anal. **9**, 371 (1962).
[12] F. C. Frank, Discuss. Faraday Soc. **25**, 19 (1958).
[13] C. W. Oseen, Trans. Faraday Soc. **29**, 883 (1933).
[14] V. Fréedericksz and V. Tsvetkov, Phys. Z. Sowjetunion **6**, 490 (1933).
[15] H. Zöcher, Trans. Faraday Soc. **29**, 945 (1933).
[16] U. Ascher and R. D. Russell, SIAM Rev. **23**, 238 (1981).
[17] L. F. Shampine, I. Gladwell, and S. Thompson, *Solving ODEs with MATLAB* (Cambridge University Press, Cambridge, England, 2003).
[18] U. M. Ascher, R. M. M. Mattheij, and R. D. Russell, *Numerical Solution of Boundary Value Problems for Ordinary Differential Equations* (SIAM, Philadelphia, 1995).
[19] E. J. Doedel, H. B. Keller, and J. P. Kernévez, Int. J. Bifurcation Chaos Appl. Sci. Eng. **1**, 493 (1991).
[20] E. J. Doedel, H. B. Keller, and J. P. Kernévez, Int. J. Bifurcation Chaos Appl. Sci. Eng. **1**, 745 (1991).
[21] K. A. Cliffe, Technical Report No. AEAT-0823, 1996 (unpublished).